NASA TECHNICAL NOTE

NASA TN D-2910

NASA TN D-2910

FLUTTER INVESTIGATION OF STREAMWISE-ORIENTED ARRAYS OF CURVED PANELS UNDER COMPRESSIVE LOADING AND AERODYNAMIC HEATING

by Robert W. Walker, Richard Rosecrans and William D. Deveikis

Langley Research Center
Langley Station, Hampton, Va.

NATIONAL AERONAUTICS AND SPACE ADMINISTRATION • WASHINGTON, D. C. • JULY 1965

NASA TN D-2910

FLUTTER INVESTIGATION OF STREAMWISE-ORIENTED ARRAYS OF CURVED PANELS UNDER COMPRESSIVE LOADING AND AERODYNAMIC HEATING

By Robert W. Walker, Richard Rosecrans,
and William D. Deveikis

Langley Research Center
Langley Station, Hampton, Va.

NATIONAL AERONAUTICS AND SPACE ADMINISTRATION

For sale by the Clearinghouse for Federal Scientific and Technical Information
Springfield, Virginia 22151 – Price $2.00

FLUTTER INVESTIGATION OF STREAMWISE-ORIENTED ARRAYS OF CURVED PANELS UNDER COMPRESSIVE LOADING AND AERODYNAMIC HEATING

By Robert W. Walker, Richard Rosecrans,
and William D. Deveikis
Langley Research Center

SUMMARY

Two large-scale cylindrical segments consisting of nine longitudinal arrays of rectangular curved panels were tested to study the flutter characteristics of panels subjected to compressive loading and aerodynamic heating. The tests were conducted at a Mach number of 3, constant dynamic pressures from 1600 to 3500 psf (77 to 168 kN/m^2), and a stagnation temperature of 300° F (422° K).

A flutter boundary was obtained which indicated that the flutter trends of the curved panels are similar to those obtained for stressed, flat panels. The influence of adjacent panels on the flutter of a given panel was found to be insignificant. The results also showed that panel curvature had a stabilizing effect relative to the minimum dynamic pressure required to initiate flutter of flat panels.

INTRODUCTION

During flight of large thin-skin launch vehicles, the curved-panel structural elements formed by ring and stringer stiffeners are often subjected to compressive loads sufficient to buckle the panels. This condition alters the stiffness of the panels and thereby may cause panel flutter. This premise is based on the flutter behavior of flat panels. For example, in references 1 to 6 it is shown that flat panels are susceptible to flutter when stressed near buckling because of a reduction in stiffness associated with the compressive loading. The subject of curved-panel flutter, particularly the flutter behavior of arrays or rows of streamwise-oriented rectangular curved panels such as those found in the cylindrical sections of current launch vehicles, has heretofore received little experimental or analytical attention.

Therefore, in view of the need for further information on curved-panel flutter, an exploratory wind-tunnel investigation was conducted in the Langley 9- by 6-foot thermal structures tunnel. The tests were designed to yield information on the effects of compressive stresses in the critical range near buckling on the flutter behavior of streamwise-oriented, curved-panel arrays under

aerodynamic heating. Also of interest was the collection of experimental evidence which might confirm the existence of a phenomenon known as cascading. Cascading is characterized by an increase in the maximum flutter amplitude in the downstream direction from one panel to the next and has been shown theoretically by Rodden for an array of streamwise-oriented flat panels (fig. 8 in ref. 7).

Two large-scale aluminum-alloy cylindrical segments containing nine arrays of streamwise-oriented rectangular curved panels of length-width ratio of approximately 2.1 were tested at a Mach number of 3. Construction of the flutter models was representative of large launch vehicles, and the test conditions simulated, as nearly as possible, the flight conditions encountered during certain portions of a typical launch trajectory. Compressive loading was primarily mechanically induced, but some thermal stresses were also present.

The data obtained in this investigation yielded a flutter boundary which shows the effects of dynamic pressure, panel stress, and buckling on curved-panel flutter. The flutter boundary is presented herein in terms of a dimensionless flutter parameter which accounts for panel geometry, material, and airflow properties.

SYMBOLS

The units used for the physical quantities defined in this paper are given in the U.S. Customary Units and in the International System of Units (SI) (ref. 8). Factors relating the two systems are given in appendix A.

A	area
C_p	pressure coefficient, $\frac{p - p_\infty}{q}$
E	Young's modulus
l	panel length
M	Mach number
P	applied compressive load
p	static pressure
p_b	static pressure in cavity under specimen
p_∞	free-stream static pressure
Δp	differential pressure acting on panels, $p_b - p_\infty$
q	free-stream dynamic pressure

ΔT temperature increase

$\beta = \sqrt{M^2 - 1}$

α coefficient of thermal expansion

σ midplane compressive stress in direction of airflow

τ panel thickness

Subscripts:

eff effective

i integer

1,2,3 stringer, panel, and skin-under-stringer element, respectively (see fig. 11)

MODELS, APPARATUS, AND TESTS

Models

Flutter models.- Two flutter models, herein designated models 1 and 2, were used in this investigation. Both models were quarter segments of a 10-foot-diameter (3.05 m) circular cylinder approximately $7\frac{1}{2}$ feet (2.3 m) long. The models were constructed of 0.032-inch-thick (0.081 cm) 2024-T4 aluminum-alloy sheet, 7075-T6 aluminum-alloy internal rings spaced 14.66 inches (37.24 cm) apart, and externally mounted hat-section longitudinal stiffeners placed at 8° intervals. The rings and stiffeners were riveted to the cylindrical skin. Spacing of the rings and stiffeners divided the skin into nine streamwise-oriented arrays of five rectangular curved panels of length-width ratio of approximately 2.1. Photographs of one of the completed models are shown as figure 1, and details of construction are given in figure 2.

Pressure model.- For this investigation, knowledge of the flow distribution over the model surface is essential in the derivation of meaningful results from data analysis. Consequently, several flow-calibration tests were conducted in which a pressure model was used. The model was constructed with externally mounted hat-section stiffeners and thus simulated the outer surface of the flutter models. It contained no internal rings but its skin thickness was greater than that of the flutter models to simplify static-orifice installation and to prevent instability. Orifices were placed in the surface so that longitudinal and transverse distributions might be surveyed.

Mounting Fixture and Hydraulic Loading System

The pressure and flutter models were installed in the mounting fixture shown in figure 3. A cross-sectional view of the fixture with model is presented in figure 4. The fixture was essentially a quarter segment of a thick-wall cylinder with a cavity approximately 3 inches (7.6 cm) deep over which the models were placed. At the upstream end was a leading-edge wedge the outer surface of which was machined parallel to the airstream. The models were mounted so that the upper surface of the hat-section stringers was flush with the surface of the leading-edge wedge. The fixture was designed to produce, as nearly as possible, uniform flow conditions over the entire model surface. In the wind-tunnel tests, the fixture was mounted to the test-section floor. A pneumatically operated sliding cover protected the models during start and shutdown of the tunnel, but during the actual test period the cover was retracted downstream. Complete retraction (or return) of the cover required between 1 and 2 seconds. The pressure in the cavity under the models was controllable.

A hydraulic loading system was used in applying compressive loads to the stringers at the downstream end of the flutter models. The upstream end of the flutter models was clamped. A separate hydraulic jack was provided for each stringer, but pressure was supplied to all the jacks through a single manifold to ensure uniform stringer loading. Each jack was calibrated individually, and variations were found to be within ±1 percent of the average value.

Instrumentation

Static-load and wind-tunnel tests were performed in this investigation. Model 1 was instrumented for both types of tests, whereas model 2 was instrumented for the wind-tunnel tests only.

Static-load tests.- Model instrumentation for the static-load tests consisted of 62 wire strain gages located on the stringers and on each panel of the center streamwise array as shown in figure 5(a). Most of the strain gages were standard, room-temperature gages not suitable for wind-tunnel use at elevated temperatures. However, where the locations were the same as those for the wind-tunnel tests, foil-type, temperature-compensated strain gages were installed and used in both types of tests. Gage circuitry consisted of a four-arm bridge with an active arm and a dummy arm.

Wind-tunnel tests.- In addition to 14 foil-type, temperature-compensated wire strain gages, model instrumentation for the wind-tunnel tests consisted of thermocouples, pressure transducers, and deflectometers. Locations of these instruments are shown in figure 5(b). For these tests, only the stringers were instrumented with strain gages. In order to avoid altering panel flutter behavior, no strain gages were mounted on the panel surfaces. Twelve iron-constantan thermocouples were spotwelded to the inner surface of the model elements. Three differential pressure transducers were used for measuring the difference in pressure at points on the model aerodynamic surface and at corresponding points in the cavity under the model, whereas absolute pressure transducers were used for measuring the cavity pressure level. A

variable-reluctance-type deflectometer located approximately $\frac{1}{4}$ inch (0.6 cm) below each curved panel in the center streamwise array and high-speed motion-picture cameras recorded panel motion. All instrumentation data were recorded with the aid of a high-speed digital magnetic-tape recording system.

Wind Tunnel

The tests were conducted in the Langley 9- by 6-foot thermal structures tunnel, an intermittent blowdown facility which operates at a Mach number of 3 and exhausts to the atmosphere. A heat exchanger provides stagnation temperatures up to 660° F (622° K). Dynamic pressures range from 1400 to 5000 pounds per square foot (67 to 239 kN/m^2). A more detailed description of the tunnel is given in reference 1.

Static-Load Tests

Inasmuch as strain-gage instrumentation was not feasible for the curved panels in the wind-tunnel tests, a method of calculation was derived for determining panel stresses. A means for testing the accuracy of the method was provided by data obtained from a number of static-load calibration tests performed on model 1. For these tests, incremental compressive loads were applied to the stringers up to and above the buckling load of the curved panels, without exceeding stringer allowable load, and strain readings were tabulated. In this manner, the distribution of mechanically induced stresses was obtained as a function of the applied stringer loads.

Strain data were recorded with the model side edges clamped and then unclamped to determine the effect of side-edge restraint on the stress distribution in various model elements. This procedure was necessary because in the wind-tunnel tests the side edges were to be clamped in order to retain proper model position in the fixture as well as to secure the model during retraction of the protective cover. Consequently, the clamped side edges constituted an artificial restraint in the sense that this condition differed from that normally expected on actual flight structures and, therefore, had to be accounted for.

Wind-Tunnel Tests

Test conditions and procedure.- The wind-tunnel tests were conducted at a Mach number of 3, constant dynamic pressures ranging from 1600 to 3500 psf (77 to 168 kN/m^2), and a stagnation temperature of 300° F (422° K). The procedure was to start the tunnel with the flutter model covered. After the desired test-section flow conditions were established, the protective cover was retracted and the pressure in the cavity under the model was adjusted to achieve stream static pressure as nearly as possible by monitoring differential-pressure-transducer output. It was important to maintain a zero pressure differential between the cavity under the model and the airstream over the model because a nonzero pressure differential would affect panel buckling. For

example, an outward differential pressure would tend to stabilize the panels and hence retard buckling, whereas an inward differential pressure would have the opposite effect. A small stringer load was applied at the start of every test in order to retain proper model position in the fixture. Additional compressive loads were then applied in increments up to and above the panel buckling load but this load was not to exceed stringer allowable load. Prior to tunnel shutdown, the compressive load was removed, and the protective cover was returned over the model.

Model surface flow distribution.- Pressure coefficients evaluated from the flow-calibration data obtained along the center line of the pressure model are shown in figure 6. These data indicate that the flow conditions along the center streamwise-oriented array of curved panels were very close to free-stream conditions. Data obtained in the transverse direction indicate that these same conditions existed along all but the two outer streamwise-oriented arrays at each side of the model. The nonuniform flow conditions along each side of the model were caused by shock-wave interference effects between the tunnel side walls and the fixture side edges.

RESULTS AND DISCUSSION

Static-Load Tests

Results from the static-load tests showed that the center-line streamwise array of panels and the array on either side of the center-line array were unaffected by model side-edge restraint. All other panels were measurably affected in shear. Typical panel and stringer stresses measured in the center arrays are plotted as a function of applied stringer load in figure 7. This variation is linear for the panel and stringer up to the panel buckling load which is seen to be between 2.25 and 2.63 kips (10.0 and 11.7 kN). As the applied loads are increased above the panel buckling load, the compressive stress abruptly increases in one surface of the panel and decreases in the other surface as expected. Accordingly, the stresses are transferred from the panel to the stringers, as shown by the increase in slope for the stringer-stress data and the decrease in slope for the panel average-stress data.

Also shown in figure 7 are calculated panel and stringer stresses. These stresses were calculated by using a method derived specifically for determining panel stresses in the wind-tunnel tests. Details of the method are explained in appendix B. This method accounts for the effect of nonuniform temperature distributions caused by aerodynamic heating for prebuckling and postbuckling loads. However, for the static-load test of figure 7, nonuniform-temperature corrections were neglected. For stresses below panel buckling, the assumption was made that all model members were subjected to the same stress. The panel prebuckling stresses, therefore, were computed by dividing the compressive loads by the cross-sectional area of the skin and the longitudinal stiffeners. The panel buckling stress was computed by using equation (11) of reference 9. For postbuckling panel stresses, panel effective areas were used. The effective area, as evaluated from figure 6.2 of reference 10, is a function of material yield stress, side-edge stress (stringer stress), and panel buckling stress.

For the calculated curves shown in figure 7 the effective area was based on the calculated panel buckling stress. Because of the interdependency of panel effective area and stringer stress, the evaluation was made with the aid of an iterative procedure.

As seen in figure 7, the measured and calculated values for panel skin and stringer are in good agreement in the prebuckling load range. However, the measured panel buckling stress is higher than the calculated value by roughly a factor of 1.5. In the panel postbuckling load range, agreement is good for the calculated and measured stringer stresses. Also, if the panel midplane stress (solid symbols) is assumed to be the average of measured stresses in both surfaces of the panel, agreement of these average stresses with the calculated panel stresses is considered fair.

Wind-Tunnel Tests

Flutter behavior.- Eleven wind-tunnel tests were performed with the two models, and in every test flutter was observed in most of the curved panels in the three center streamwise arrays. However, the panels did not flutter in any discernible order; rather, they appeared to flutter on an individual basis and, to a great extent, they were unaffected by the behavior of adjacent panels - that is, there was no evidence of cascading. High-speed motion pictures showed that, when one panel was in a pronounced state of flutter, there was often a slight related motion of one or more adjacent panels, but this effect was small, sometimes intermittent, and not sufficiently consistent to be conclusive. Also, no systematic order to start or stop of panel flutter could be discerned. No panel was consistently more prone to start or stop fluttering than any other. The behavior of any particular panel probably would be affected by the action of nearby panels if the rings and stringers were more flexible, but such a conclusion could not be established by the present tests. The flutter motion was not violent enough to cause any noticeable damage to any of the panels in the center streamwise arrays even after the total accumulated flutter time from repeated tests reached 1 minute. Cracks appeared in two panels located along the sides of the models in the region of high shear stress and disturbed airflow after repeated tests with a total accumulated flutter time of 1 to 2 minutes.

Flutter results.- Curved-panel flutter results from all tests are presented in figure 8 in terms of the nondimensional flutter parameter $\left(\frac{\beta E}{q}\right)^{1/3}\frac{\tau}{l}$ and the calculated panel stress. The data points represent the first observed start of flutter (open symbols) and the last observed stop of flutter (solid symbols) in the center array; all intermediate flutter start and stop points have been omitted. Test conditions corresponding to the flutter points are given in table I. The solid curves in the figure are boundaries faired through the data. These curves converge to a common point and indicate overall trends similar to those of stressed, flat panels. (See, for example, refs. 1 to 6.) For flat panels, this common point has been referred to as the transition point because it denotes the transition between unbuckled and buckled regions - that is, for stresses less than the transition-point stress, the flat panels were unbuckled

and for stresses greater than the transition-point stress, they were buckled. For the curved panels of the present investigation, it was not possible to determine with certainty the panel condition when flutter started and stopped. However, it seems reasonable to assume on the basis of flat-panel results, that the curved panels were unbuckled when flutter started and buckled when flutter stopped. The panel stresses shown in figure 8 were thus calculated on the basis of these assumptions. In figure 8, the transition-point stress is approximately twice the average experimental static or no-flow buckling stress denoted by the tick mark. This apparent suppression of buckling in the presence of supersonic flow has been supported theoretically (for example, refs. 5 and 11), and has been observed experimentally for flat panels (ref. 6). Thus, as is true for flat panels, the flutter of curved panels is dependent upon dynamic pressure and panel stress oriented in the flow direction. The dynamic pressure required to initiate flutter decreases to a minimum as panel stresses increase up to the transition-point stress; as panel stresses exceed the transition-point stress, however, the required dynamic pressure increases. Hence, with respect to the minimum dynamic pressure required for flutter, panel stresses substantially above or below the transition-point stress tend to stabilize the panels.

The flutter region of the two models tested in this investigation has been defined, as shown by the data in figure 8, at least within the operating range of the Langley 9- by 6-foot thermal structures tunnel. The results obtained from the two models differed somewhat, presumably because of small differences in fabrication. Consequently, it may be assumed that if more models were tested, the flutter region might be changed. The figure indicates that there is a value of the flutter parameter above which the panels will not flutter. This critical value appears to be in the neighborhood of 0.32 to 0.34 for the particular size and shape of panels studied in the present tests. For similar tests of flat panels of the same size, shape, and material as those of the present investigation, flutter occurred at a flutter-parameter value of 0.46. (See ref. 2.) Such a large difference indicates that the panel curvature had a considerable stabilizing effect.

Calculated panel stresses.- Inasmuch as the curved-panel elements of the wind-tunnel models contained no strain-gage instrumentation, panel stresses due to applied stringer stresses and aerodynamic heating were evaluated by means of a calculating procedure. Neither the effects due to a nonzero pressure differential between stream pressure and cavity pressure under the model nor any other airflow effects were accounted for in this procedure. The calculated panel stresses depend only on applied stringer load, temperature increases in various model elements, and element geometry. The applied stringer loads were obtained from records of the variation of load with time, such as that for test 1 shown in figure 9. Nonuniform temperature corrections, provided for in the calculating procedure, were made with the aid of temperature histories such as that shown for test 1 in figure 10 for stringer, panel, and skin beneath the stringer.

The actual skin and stringer areas, defined in figure 11, were used in equations (10) to (12) of appendix B to compute panel stresses for the flutter-start points in order to comply with the assumption that the panels were unbuckled at start of flutter. For the flutter-stop points, panel effective areas were used in equation (13) of appendix B. The panel buckling stress, used in

the evaluation of effective areas, had to be assumed in the absence of a method for accurately determining this stress. Consequently, the highest flutter-start stress (10 ksi (69.0 MN/m^2), see table I, test 1) was used as a first approximation of the panel buckling stress.

Stringer stresses were then computed and compared with values determined from stringer strain-gage measurements to check the validity of using the assumed panel buckling stress in the method of calculation. Typical variations of computed and measured stresses with time are shown in figure 12 (test 1). The solid curve represents the calculated stringer stresses. Discontinuities in the curve and data (symbols) reflect load-curve discontinuities (fig. 9). For applied stringer loads up to the load required to produce the assumed panel buckling stress of 10 ksi (69.0 MN/m^2) actual elemental areas (see fig. 11) were used in the computation of stringer stresses (eqs. (11), (12), and (13) in appendix B). For greater values of applied stringer load, panel effective areas were used. During the early part of the test when applied load was small, agreement between test and computed values is poor; during later parts of the test when applied loads were appreciable (and when flutter data were obtained), the agreement is considered fair to good. Hence, inasmuch as calculated and measured stresses for both the panel and the stringer with no airflow were in good agreement (fig. 7) and those for the stringer with airflow were at least in fair agreement, the calculated panel stresses with airflow can be assumed to be representative. The method of calculation did not include effects of pressure differential but did include the assumption that the panel was not buckled at the start of flutter. However, the measured values of differential pressure were small and, consequently, the calculated panel stresses should be fairly good for the flutter-start points.

CONCLUDING REMARKS

Two large-scale ring- and stringer-stiffened cylindrical segments consisting of nine longitudinal arrays of rectangular curved panels were tested in the Langley 9- by 6-foot thermal structures tunnel to study the effects of compressive stress on flutter of curved panels exposed to aerodynamic heating. Attention was directed at the critical range of stresses near panel buckling. Also of interest was the collection of experimental evidence which might confirm the existence of the cascading phenomenon. The tests were conducted at a Mach number of 3, constant dynamic pressures from 1600 to 3500 psf (77 to 168 kN/m^2), and a stagnation temperature of 300° F (422° K).

The panels appeared to flutter on an individual basis and were unaffected by the behavior of adjacent panels - that is, there was no evidence of cascading. However, the behavior of adjacent panels probably would have been significant had the rings and stringers been more flexible. A flutter boundary was established from test data which indicated overall trends similar to those

of stressed, flat panels. The test results showed that panel curvature has a stabilizing effect relative to the minimum dynamic pressure required for flutter of flat panels.

Langley Research Center,
National Aeronautics and Space Administration,
Langley Station, Hampton, Va., March 26, 1965.

APPENDIX A

CONVERSION OF U.S. CUSTOMARY UNITS TO SI UNITS

The International System of Units (SI) was adopted by the Eleventh General Conference on Weights and Measures held in Paris, October 1960, in Resolution No. 12 (ref. 8). Conversion factors required for units used herein are given in the following table:

Physical quantity	U.S. customary unit	Conversion factor (*)	SI unit
Length	in.	0.0254	meters (m)
	ft	0.3048	meters (m)
Load	kips	4.448×10^3	newtons (N)
	lb	4.448	newtons (N)
Pressure	psi	6.895×10^3	newtons/meter^2 (N/m^2)
	psf	47.88	newtons/meter^2 (N/m^2)
Stress	ksi	6.895×10^6	newtons/meter^2 (N/m^2)
Temperature	($^\circ$F + 460)	5/9	degrees Kelvin ($^\circ$K)

*Multiply value given in U.S. customary unit by conversion factor to obtain equivalent value in SI unit.

Prefixes to indicate multiples of units are as follows:

Prefix	Multiple
centi (c)	10^{-2}
giga (G)	10^9
hecto (h)	10^2
kilo (k)	10^3
mega (M)	10^6

APPENDIX B

STRESS CALCULATIONS

A typical model section used in the calculation of stresses is shown in figure 11. The section is divided into three elements which are subjected to uniform compressive loads (P_1, P_2, and P_3) and temperature increases (ΔT_1, ΔT_2, and ΔT_3). Inasmuch as the three elements are attached, the final elongation or shortening δ of each element due to the compressive loads and temperature increases is assumed to be the same, and therefore the following equations can be written for the three elements:

$$\alpha \Delta T_1 l - \frac{P_1 l}{A_1 E} = \delta \tag{1}$$

$$\alpha \Delta T_2 l - \frac{P_2 l}{A_2 E} = \delta \tag{2}$$

$$\alpha \Delta T_3 l - \frac{P_3 l}{A_3 E} = \delta \tag{3}$$

Subtracting equation (1) from equation (2) and equation (1) from equation (3) and letting

$$P = P_1 + P_2 + P_3 \tag{4}$$

and

$$\sigma_i = \frac{P_i}{A_i} \tag{5}$$

yields

$$\sigma_2 - \sigma_1 = \frac{P_2}{A_2} - \frac{P - P_2 - P_3}{A_1} = \alpha E\left(\Delta T_2 - \Delta T_1\right) \tag{6}$$

$$\sigma_3 - \sigma_1 = \frac{P_3}{A_3} - \frac{P - P_2 - P_3}{A_1} = \alpha E\left(\Delta T_3 - \Delta T_1\right) \tag{7}$$

From whence the following can be obtained:

$$\sigma_2\left(1 + \frac{A_2}{A_1}\right) - \frac{P}{A_1} + \sigma_3 \frac{A_3}{A_1} = \alpha E\left(\Delta T_2 - \Delta T_1\right) \tag{8}$$

$$\sigma_3\left(1 + \frac{A_3}{A_1}\right) - \frac{P}{A_1} + \sigma_2 \frac{A_2}{A_1} = \alpha E\left(\Delta T_3 - \Delta T_1\right) \tag{9}$$

The simultaneous solution of equations (8) and (9) yields the following expressions for σ_2 and σ_3:

$$\sigma_2 = \frac{\frac{P}{A_1} - \alpha E\left[\left(\Delta T_3 - \Delta T_2\right)\frac{A_3}{A_1} - \left(\Delta T_2 - \Delta T_1\right)\right]}{1 + \frac{A_2}{A_1} + \frac{A_3}{A_1}} \tag{10}$$

$$\sigma_3 = \frac{\frac{P}{A_1} + \alpha E\left[\left(\Delta T_3 - \Delta T_2\right)\frac{A_2}{A_1} + \left(\Delta T_3 - \Delta T_1\right)\right]}{1 + \frac{A_2}{A_1} + \frac{A_3}{A_1}} \tag{11}$$

Then, by substituting equation (10) into equation (6) or equation (11) into equation (7) the following equation for σ_1 is obtained:

$$\sigma_1 = \frac{\frac{P}{A_1} - \alpha E\left[\left(\Delta T_2 - \Delta T_1\right)\frac{A_2}{A_1} + \left(\Delta T_3 - \Delta T_1\right)\frac{A_3}{A_1}\right]}{1 + \frac{A_2}{A_1} + \frac{A_3}{A_1}} \tag{12}$$

From equations (10), (11), and (12), stresses in the elements are obtained from the known total applied compressive loads and temperature increases of the elements. When the skin is buckled, A_2 is replaced with $A_{2,eff}$ in equations (11) and (12), and from equations (5) and (10) σ_2 becomes

$$\sigma_2 = \frac{A_{2,eff}}{A_2}\left\{\frac{\frac{P}{A_1} - \alpha E\left[\left(\Delta T_3 - \Delta T_2\right)\frac{A_3}{A_1} - \left(\Delta T_2 - \Delta T_1\right)\right]}{1 + \frac{A_{2,eff}}{A_1} + \frac{A_3}{A_1}}\right\} \tag{13}$$

REFERENCES

1. Dixon, Sidney C.; Griffith, George E.; and Bohon, Herman L.: Experimental Investigation at Mach Number 3.0 of the Effects of Thermal Stress and Buckling on the Flutter of Four-Bay Aluminum Alloy Panels With Length-Width Ratios of 10. NASA TN D-921, 1961.

2. Hess, Robert W.; and Gibson, Frederick W.: Experimental Investigation of the Effects of Compressive Stress on the Flutter of a Curved Panel and a Flat Panel at Supersonic Mach Numbers. NASA TN D-1386, 1962.

3. Dixon, Sidney C.: Experimental Investigation at Mach Number 3.0 of Effects of Thermal Stress and Buckling on Flutter Characteristics of Flat Single-Bay Panels of Length-Width Ratio 0.96. NASA TN D-1485, 1962.

4. Dixon, Sidney C.; and Shore, Charles P.: Effects of Differential Pressure, Thermal Stress, and Buckling on Flutter of Flat Panels With Length-Width Ratio of 2. NASA TN D-2047, 1963.

5. Dixon, Sidney C.: Application of Transtability Concept to Flutter of Finite Panels and Experimental Results. NASA TN D-1948, 1963.

6. Guy, Lawrence D.; and Bohon, Herman L.: Flutter of Aerodynamically Heated Aluminum-Alloy and Stainless-Steel Panels With Length-Width Ratio of 10 at Mach Number of 3.0. NASA TN D-1353, 1962.

7. Fung, Y. C. B.: A Summary of the Theories and Experiments on Panel Flutter. AFOSR TN 60-224, Guggenheim Aeron. Lab., C.I.T., May 1960. (Available from ASTIA as AD 240284.)

8. Mechtly, E. A.: The International System of Units - Physical Constants and Conversion Factors. NASA SP-7012, 1964.

9. Peterson, James P.; and Whitley, Ralph O.: Local Buckling of Longitudinally Stiffened Curved Plates. NASA TN D-750, 1961.

10. Sechler, Ernest E.; and Dunn, Louis G.: Airplane Structural Analysis and Design. John Wiley & Sons, Inc., 1942, p. 205.

11. Houbolt, John C.: A Study of Several Aerothermoelastic Problems of Aircraft Structures in High-Speed Flight. Nr. 5, Mitteilungen aus dem Institut für Flugzeugstatik und Leichtbau, Leemann (Zürich), c.1958.

TABLE I.- FLUTTER RESULTS FOR CURVED PANELS

[Material: 2024-T4 aluminum alloy; E = 10.6×10^6 psi (73.1 GN/m^2)]

Test	Model	Free-stream dynamic pressure, q		Flutter parameter, $\left(\frac{\beta E}{q}\right)^{1/3} \frac{\tau}{l}$	Differential pressure, Δp		Flutter start				Flutter stop			
							Stringer compressive load		Calculated panel compressive stress		Stringer compressive load		Calculated panel compressive stress	
		psf	kN/m^2		psf	hN/m^2	lb	kN	ksi	MN/m^2	lb	kN	ksi	MN/m^2
1	1	1630	78	0.306	7	3	4120	18.3	10.000	69.0	4875	21.7	10.825	74.6
2	1	2120	102	.280	0	0	3520	15.6	9.800	67.6	5620	25.0	12.300	84.8
3	1	2490	119	.265	-7	-3	3370	15.0	9.580	66.1	6000		12.700	87.6
4	1	3000	144	.250	0	0	3450	15.3	9.230	63.6		26.7		
5	1	3480	167	.238	14	7	3000	13.3	8.190	56.5				
6	2	1660	79	.305	0	0	3000	13.3	9.650	66.5				
7	2	2140	102	.280	-12	-6	2480	11.0	8.200	56.5	5180	23.0	11.900	82.1
8	2	2520	121	.265	7	3	3200	14.2	8.400	57.9	5020	22.3	10.950	75.5
9	2	3000	144	.250	-22	-11	3000	13.3	7.700	53.1	5780	25.7	12.150	83.8
10	2	3480	167	.238	-29	-14	2320	10.3	8.450	58.3				
11	2	2490	119	.265	7	3	2400	10.7	7.750	53.4	5550	24.7	11.975	82.6

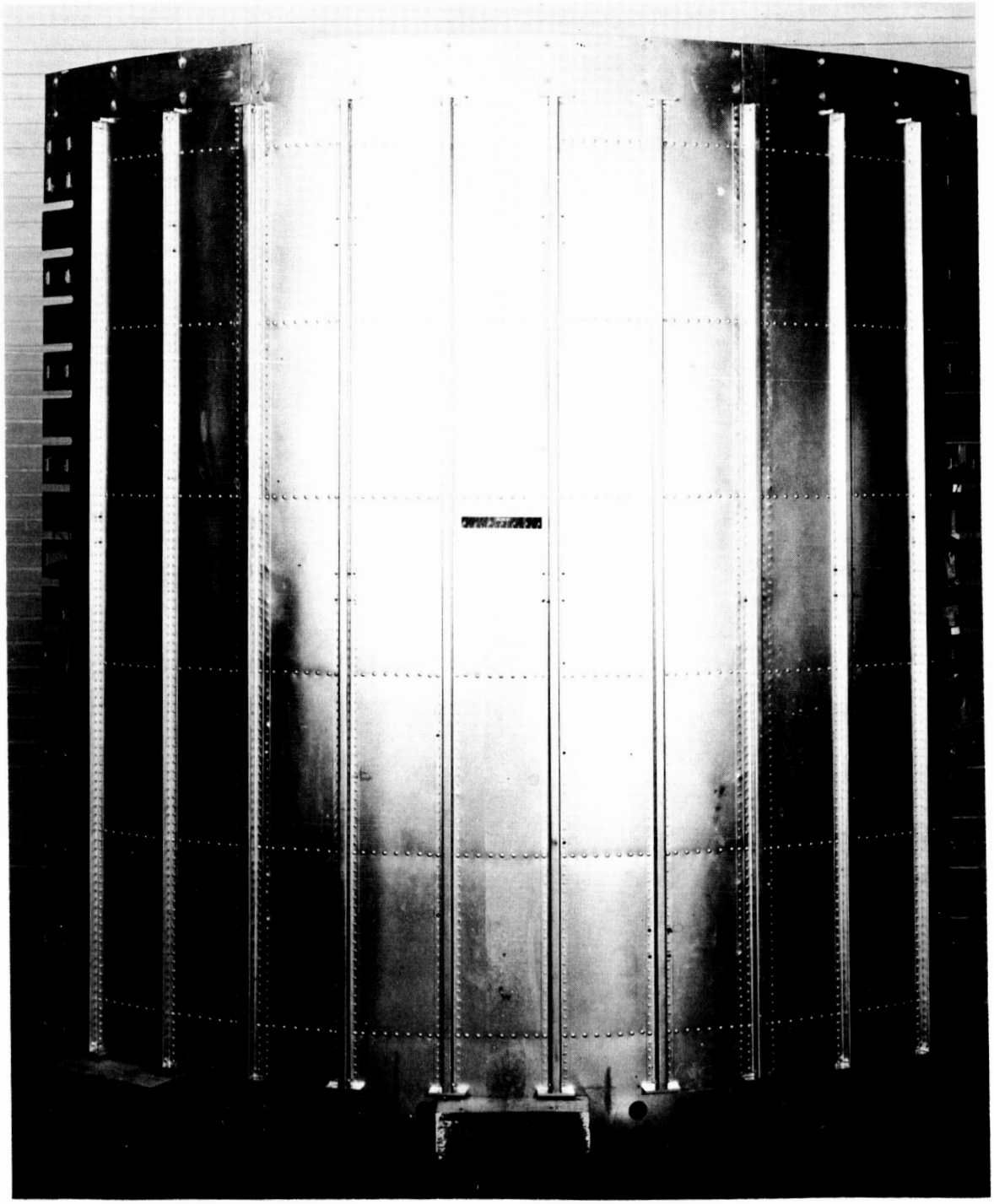

(a) Outer surface. L-63-1095.1

Figure 1.- Flutter model used in investigation.

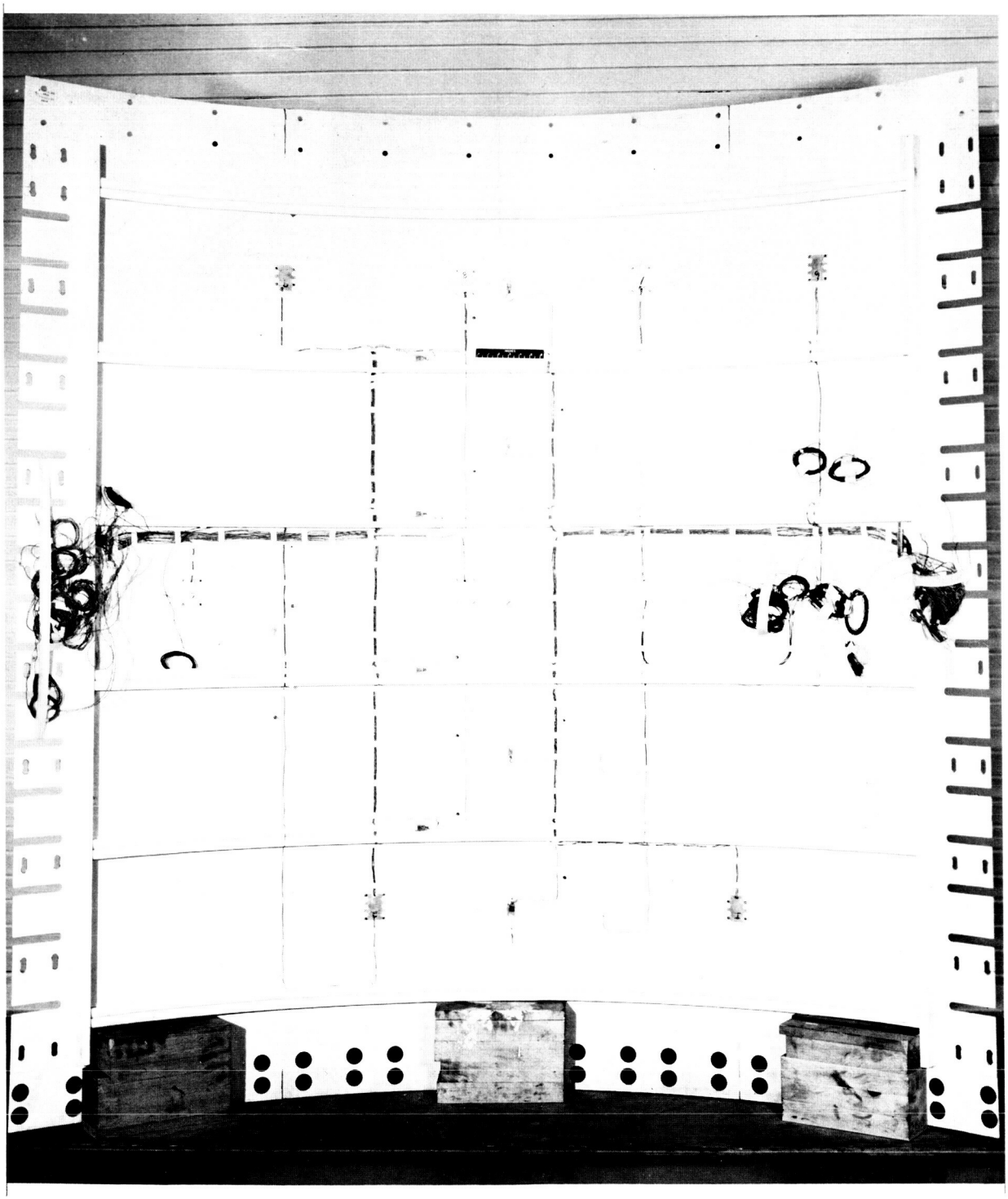

(b) Inner surface. L-63-1096.1

Figure 1.- Concluded.

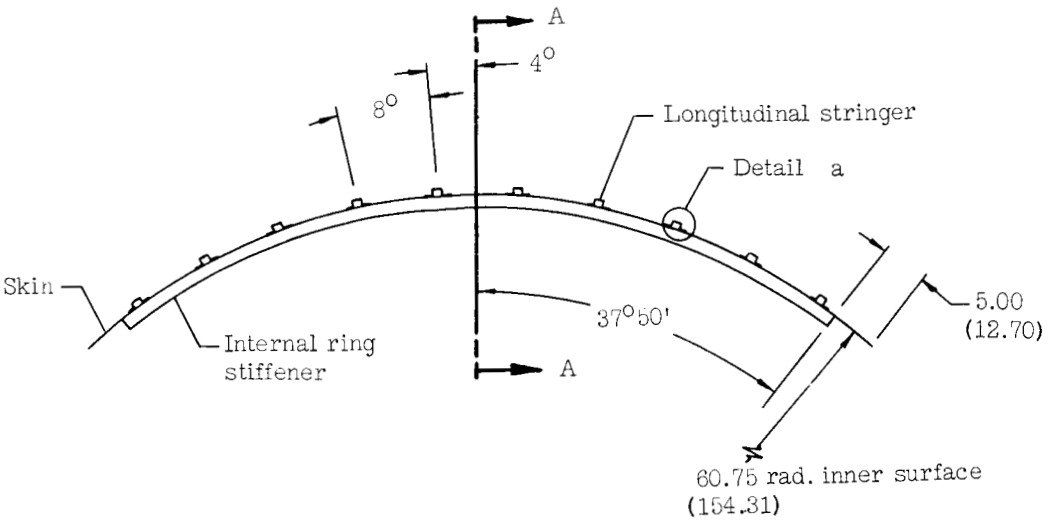

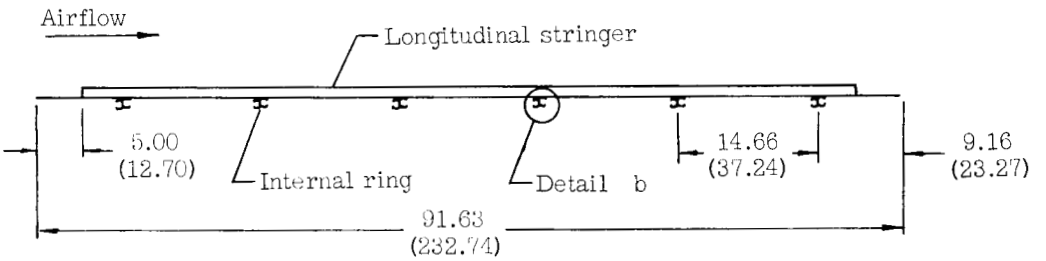

Section A-A

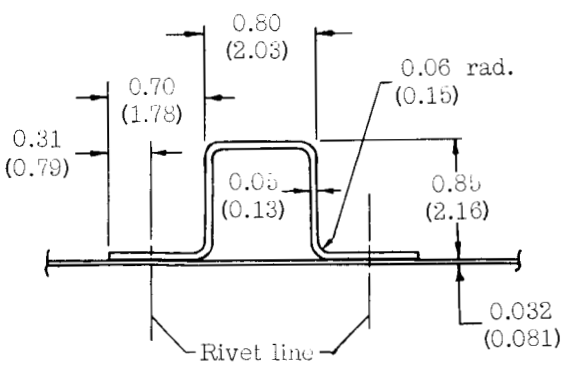

Detail a

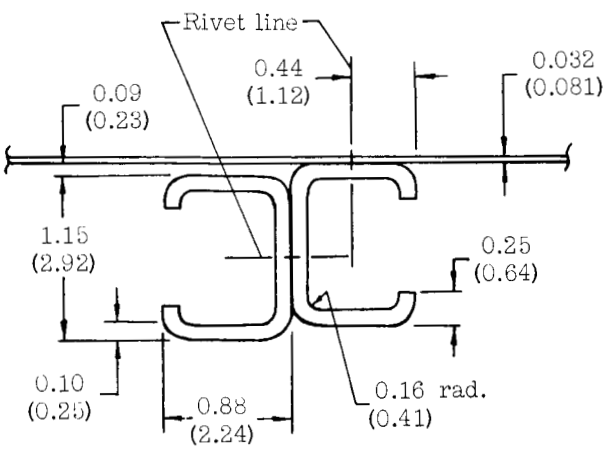

Detail b

Figure 2.- Specimen construction details. End view of specimen. Dimensions in parentheses are in centimeters; all other dimensions are in inches.

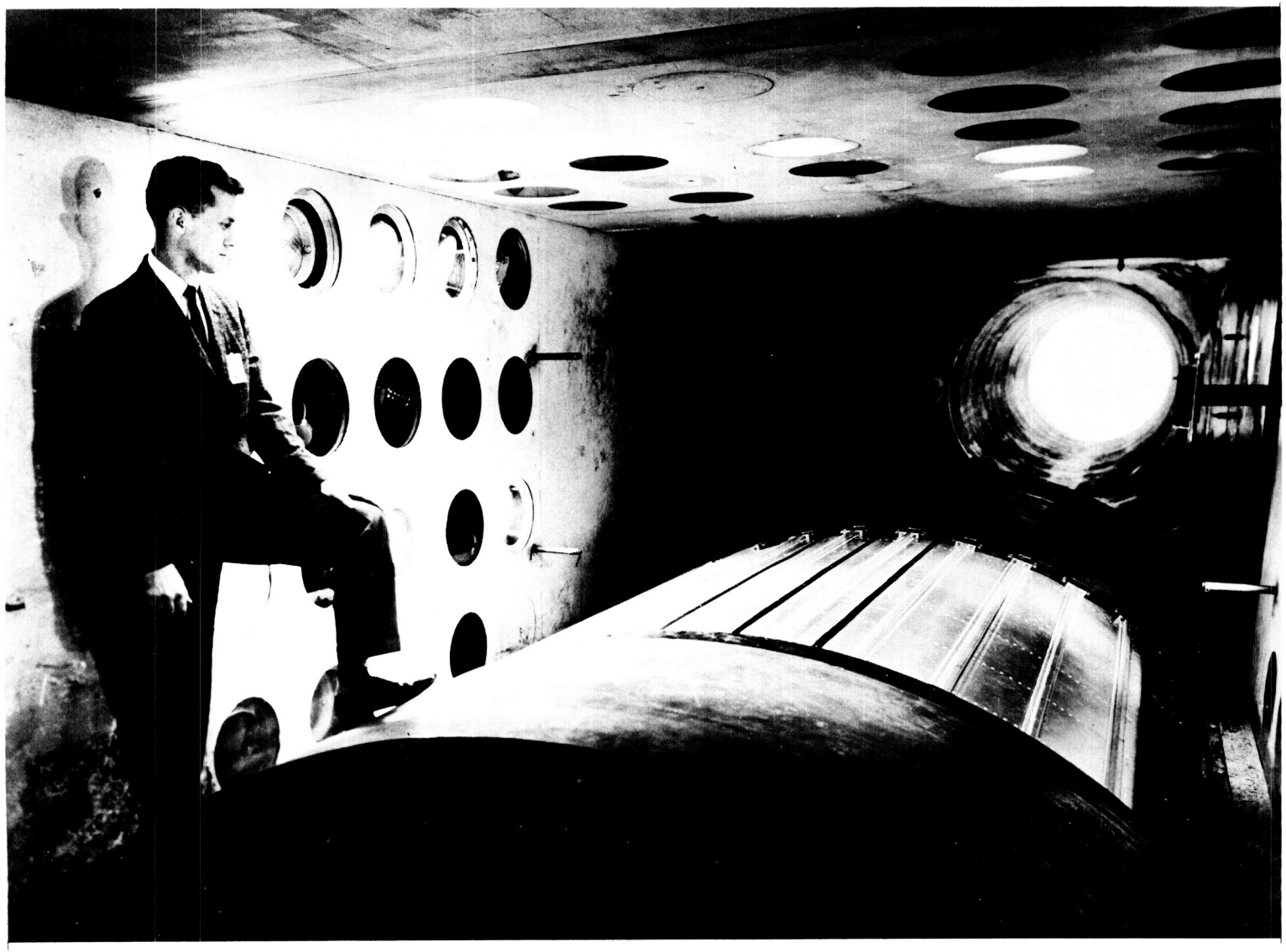

L-62-8672

Figure 3.- Mounting device in tunnel test section with model installed as viewed from upstream. Protective cover in retracted position.

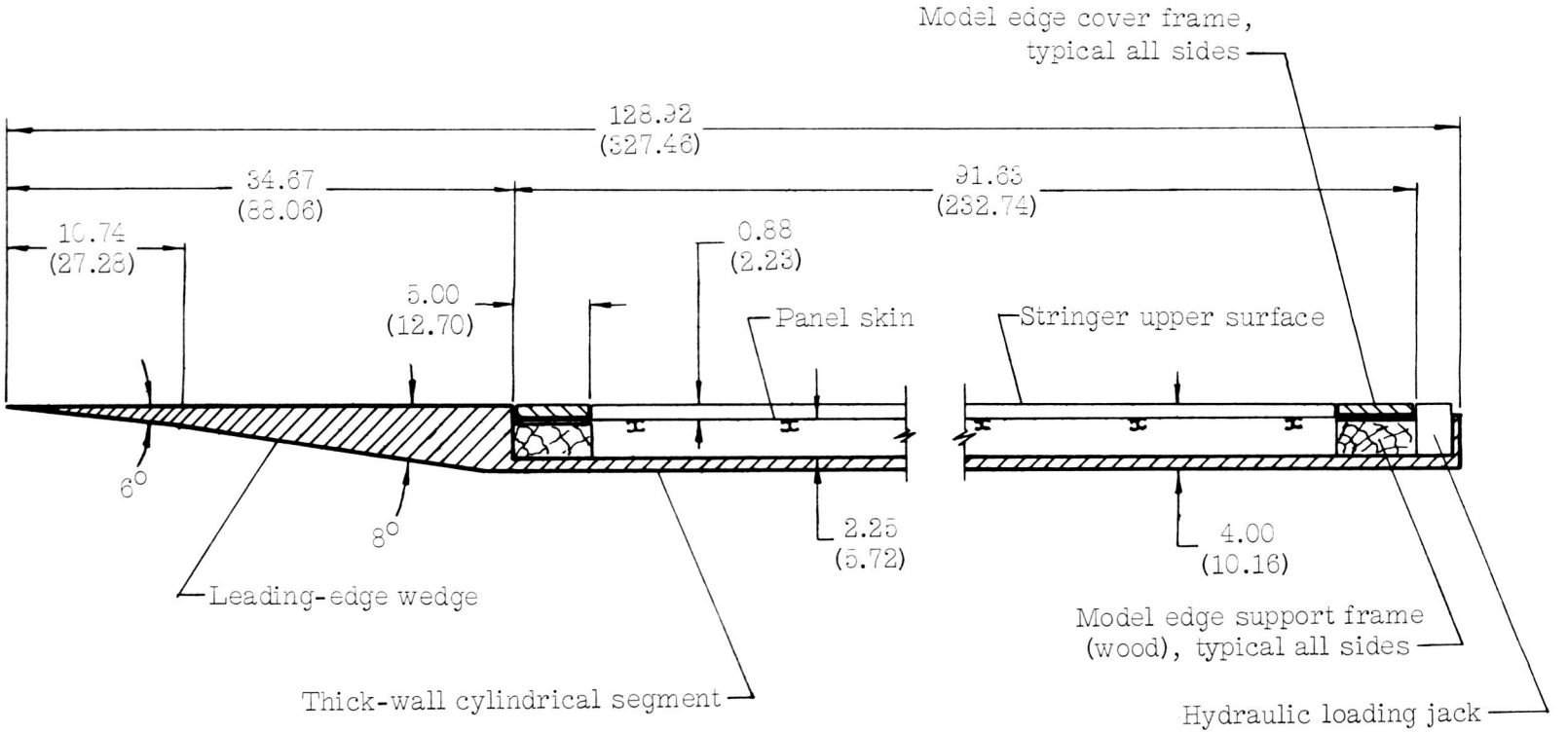

Figure 4.- Cross-sectional view of mounting fixture with model in place. Retractable protective cover not shown. Dimensions in parentheses are in centimeters; all other dimensions are in inches.

○ Two strain gages, one on each side of panel

□ Two strain gages, one on each side of longitudinal stringer

◇ Three strain gages, one on each side of longitudinal stringer plus one on skin under stringer

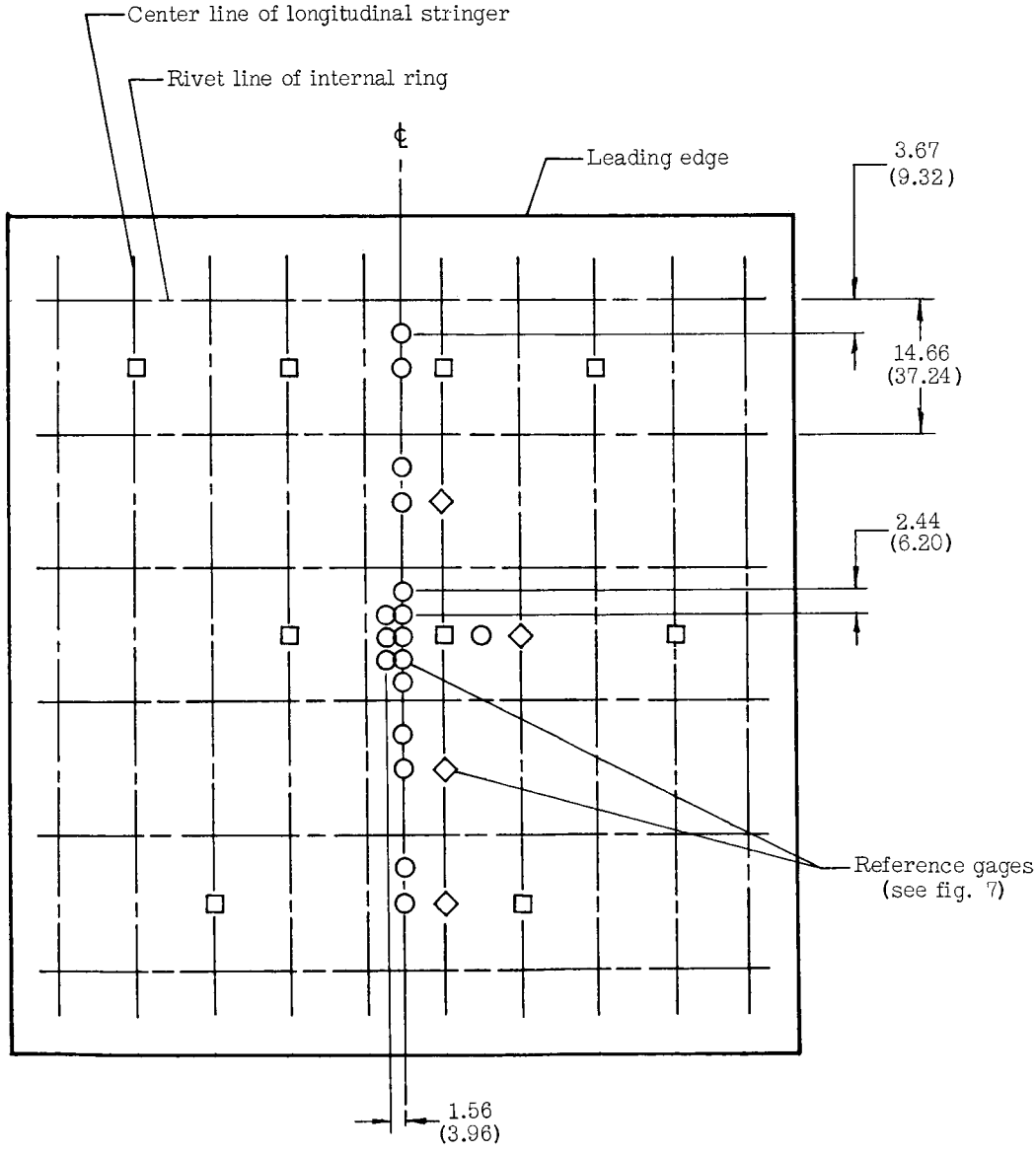

(a) Static-load tests.

Figure 5.- Model instrumentation. Top view of specimen (flattened out). Dimensions in parentheses are in centimeters; all other dimensions are in inches.

○ Variable-reluctance deflectometer

□ Two strain gages, one on each side of longitudinal stringer

◇ Thermocouple attached to panel

△ Thermocouple attached to longitudinal stringer

◺ Five thermocouples attached at different locations on longitudinal stringer and skin under stringer

◺ Differential pressure gage

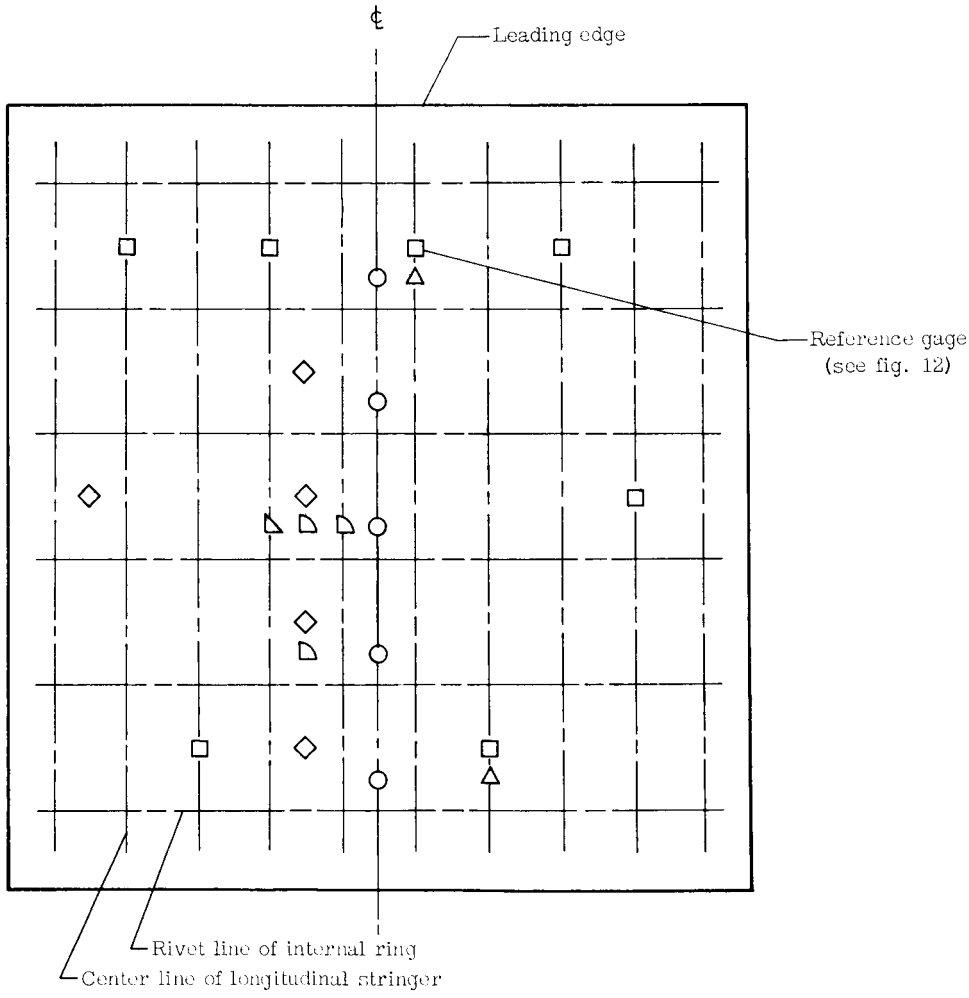

(b) Wind-tunnel tests.

Figure 5.- Concluded.

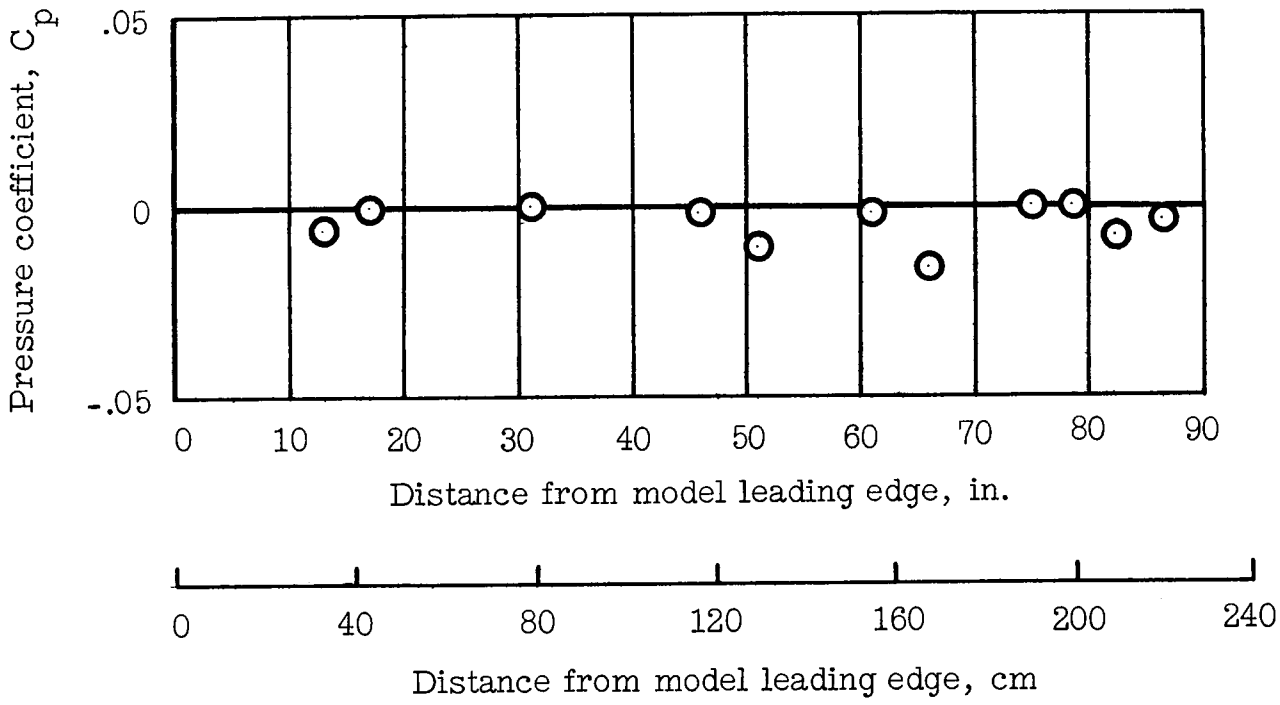

Figure 6.- Longitudinal pressure distribution along pressure-model center line.

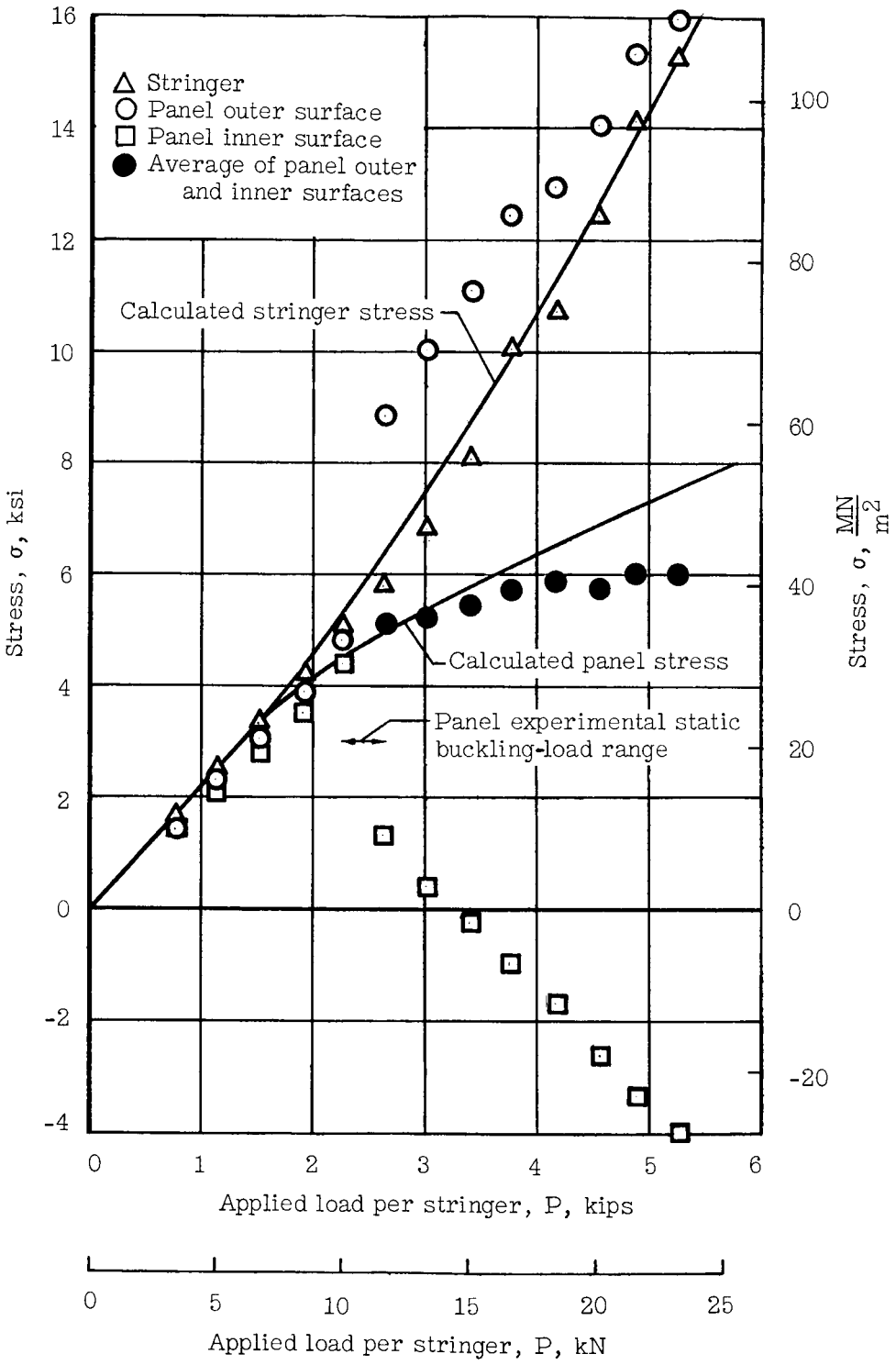

Figure 7.- Typical measured and calculated stresses from a static-load test plotted as a function of applied stringer load. Positive values denote compression.

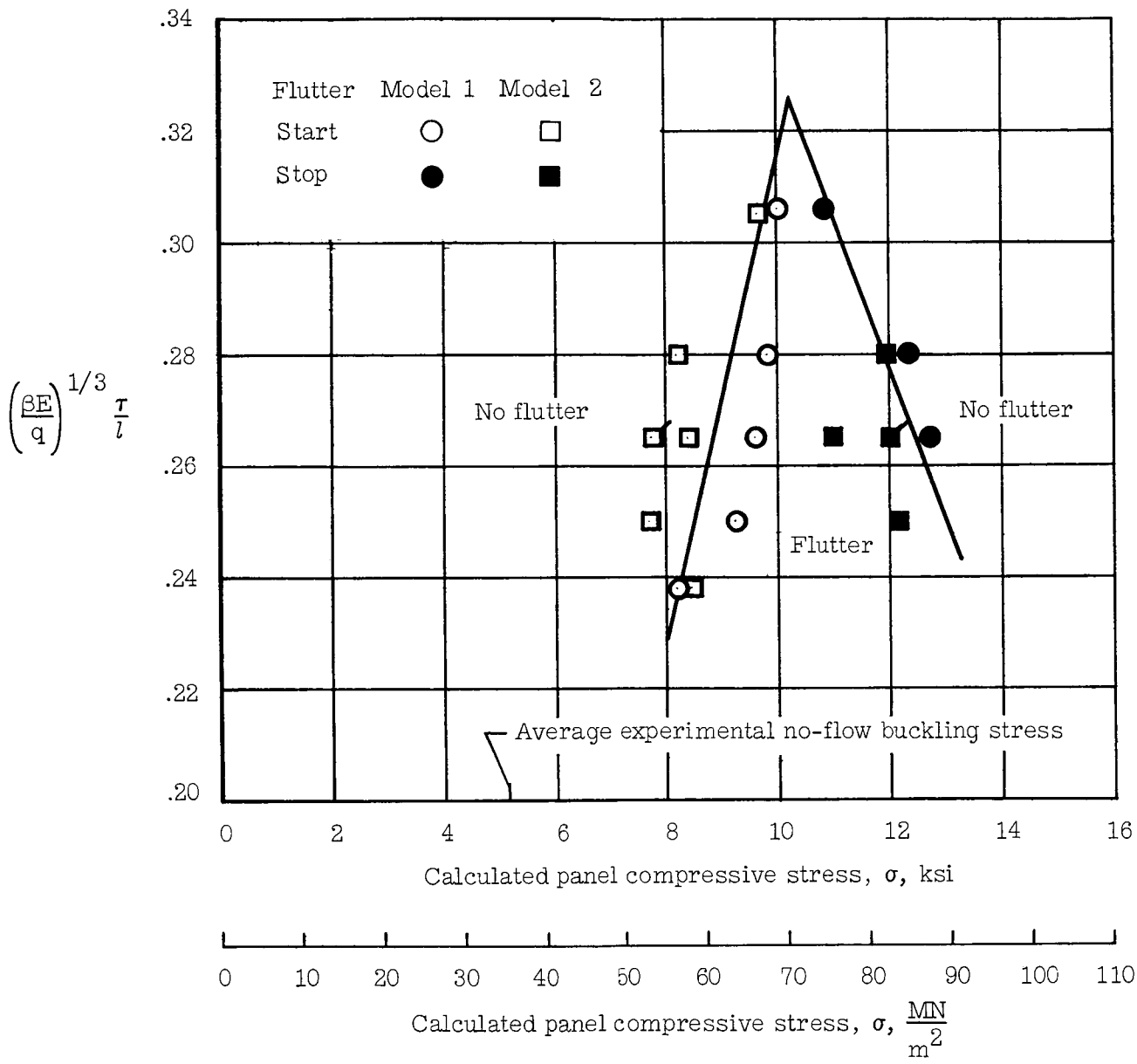

Figure 8.- Effect of panel compressive stress on flutter of curved panels. Flagged symbols denote repeat test points.

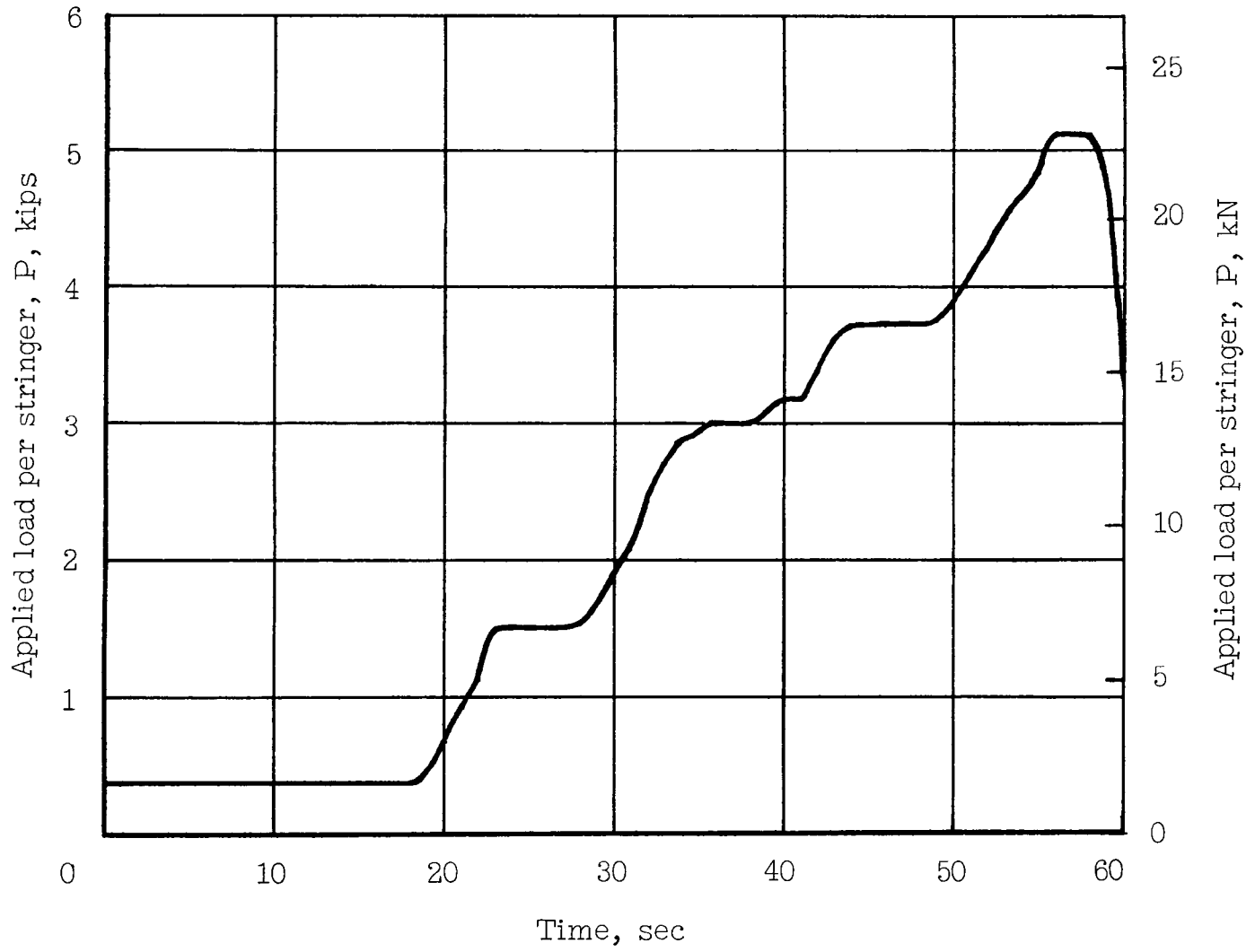

Figure 9.- Typical variation of applied stringer load with time during wind-tunnel tests. Test 1.

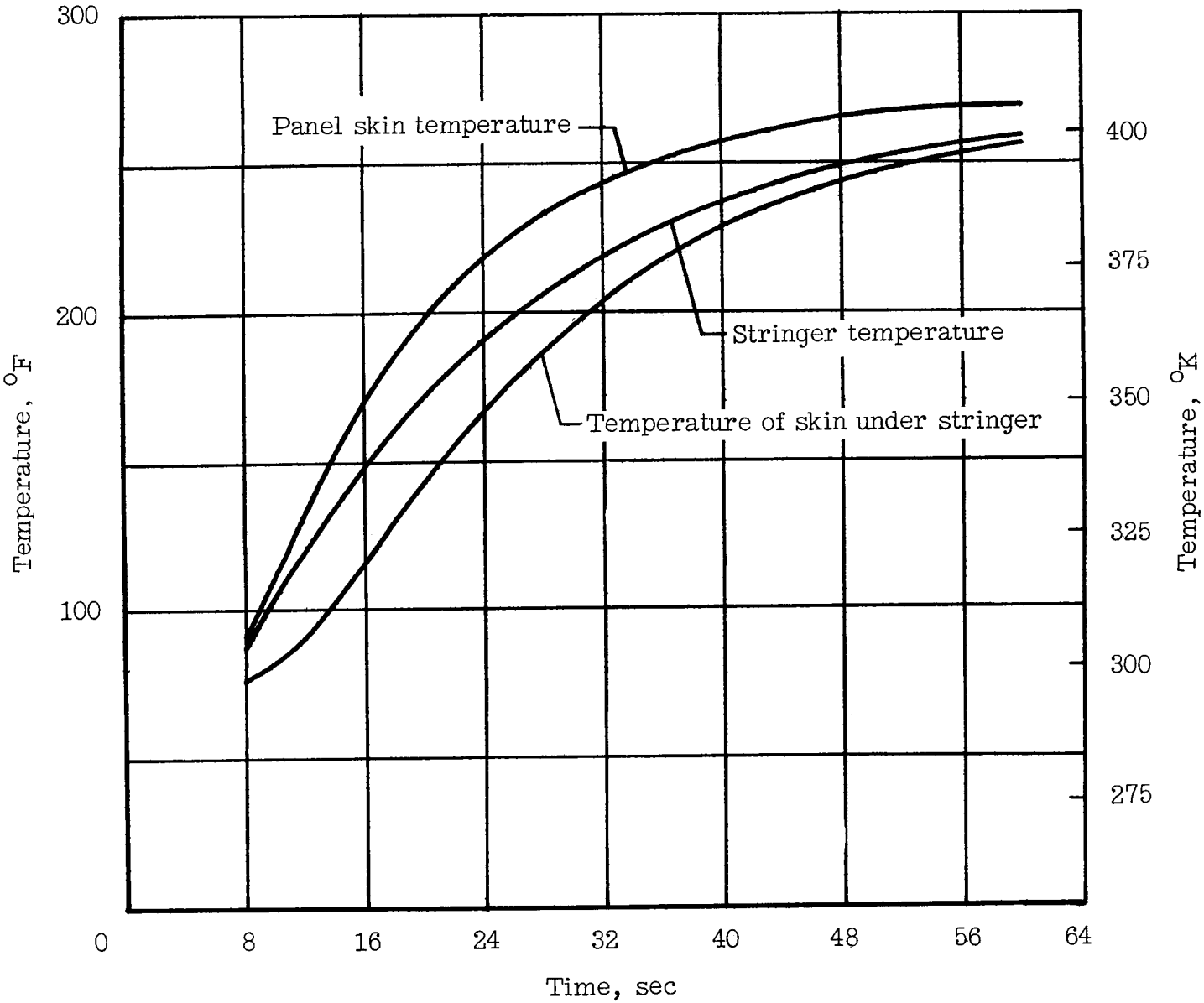

Figure 10.- Typical model temperature variations during wind-tunnel tests. Test 1.

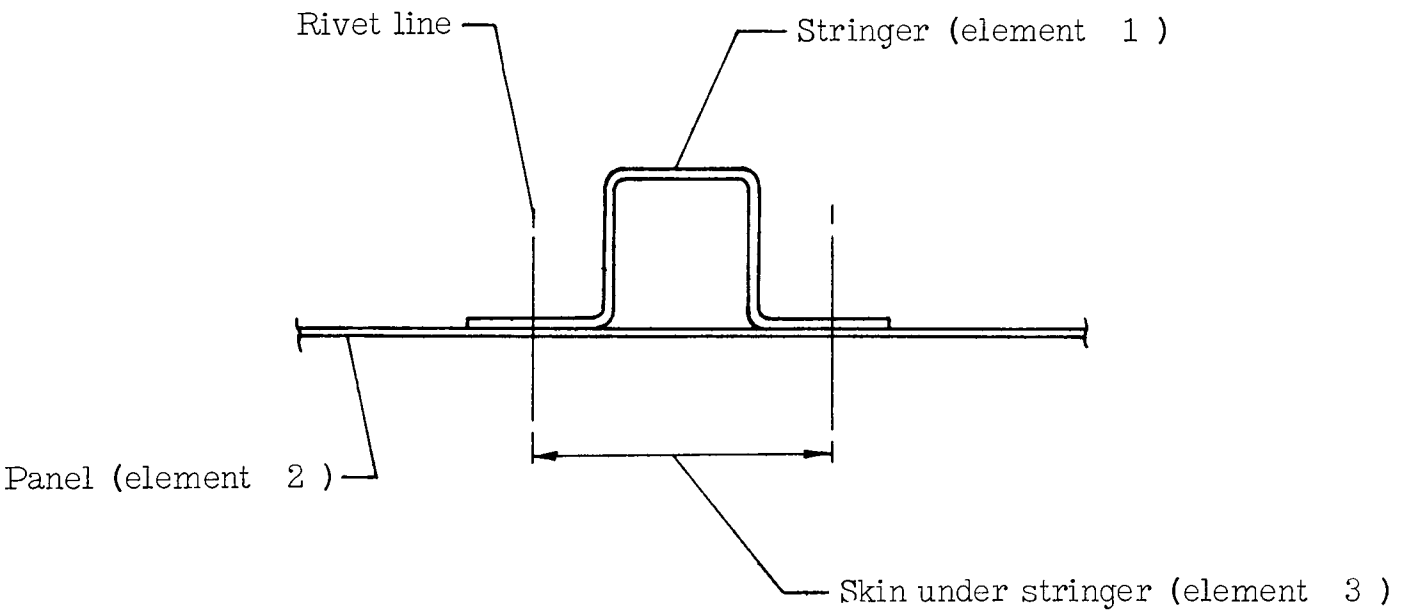

Figure 11.- End view of typical longitudinal stringer and corresponding skin.

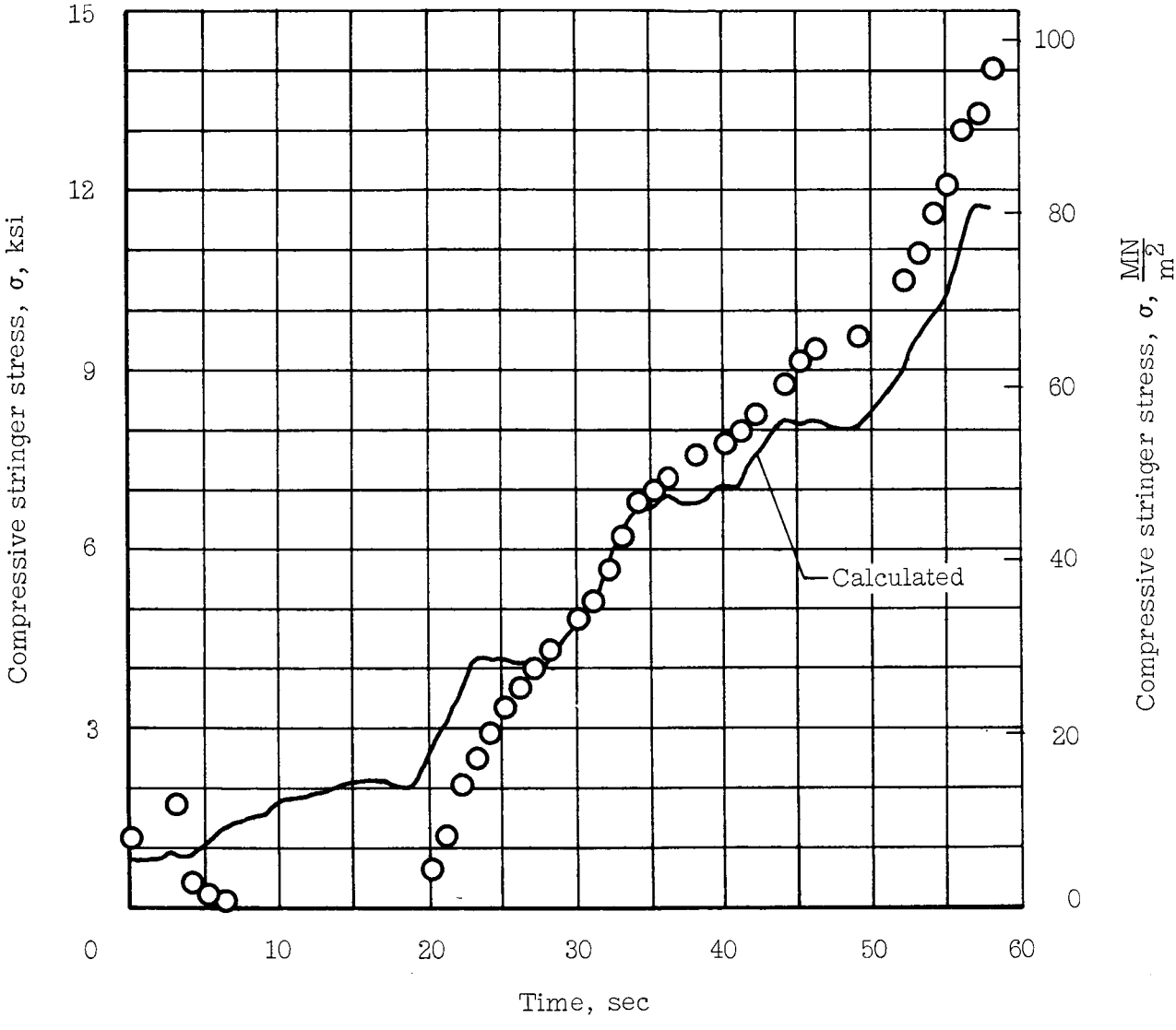

Figure 12.- Measured and calculated variations of stringer stress with time during wind-tunnel tests. Test 1.